JOURNAL OF AIRCRAFT
Vol. 35, No. 3, May–June 1998

Power Requirements for Large-Amplitude Flapping Flight

Kenneth C. Hall* and Steven A. Pigott†
Duke University, Durham, North Carolina 27708-0300
and
Steven R. Hall‡
Massachusetts Institute of Technology, Cambridge, Massachusetts 02139-4307

In this paper, a method is presented for computing the circulation distribution along the span of a flapping wing that minimizes the power required to generate a prescribed lift and thrust. The power is composed of three parts: useful thrust power, induced power, and profile power. Here, the thrust and induced power are expressed in terms of the Kelvin impulse and kinetic energy associated with the sheet of trailing and shed vorticity left behind the flapping wing. The profile power is computed using a quasisteady approximation of the two-dimensional viscous drag polar at each spanwise station of the wing. A variational principle is then formed to determine the necessary conditions for the circulation distribution to be optimal. Included in the variational principle is a constraint that the wing not stall. This variational principle, which is essentially the viscous extension of the well-known Betz criterion for optimal propellers, is discretized using a vortex-lattice model of the wake, and the optimum solution is computed numerically. The present method is used to analyze a conventional propeller as well as a rigid wing in forward-flight flapping about a hinge point on the longitudinal axis.

Nomenclature

$\mathcal{A}$ = surface bounding Trefftz volume $\mathcal{V}$
B = matrix relating circulation Γ to force F
b = wingspan
$\boldsymbol{b}_j$ = jth row of B
C_d, C_l = sectional drag and lift coefficients
C_{d0}, C_{d2} = parameters of drag coefficient curve fit
$C_{\mathcal{L}_1}$, $C_{\mathcal{T}_1}$, $C_{\mathcal{P}}$ = coefficients of lift, thrust, and power
C_{l0} = sectional lift coefficient at minimum sectional drag
$C_{\mathcal{P}_0}$ = coefficient of power required for steady gliding flight
c = aerodynamic chord
d = sectional drag
$\boldsymbol{F}$ = time-averaged aerodynamic force vector
$\boldsymbol{i}$, $\boldsymbol{j}$, $\boldsymbol{k}$ = unit vectors in the x, y, and z directions
K = induced power matrix
k = reduced frequency, $\Omega b/U$
$\mathcal{L}_1$ = time-averaged aerodynamic lift
l = sectional lift
N = number of vortex ring panels in wake model
$\boldsymbol{n}$ = unit vector normal to wake
$\boldsymbol{n}_j$ = unit vector normal to jth vortex panel
$\mathcal{P}$ = time-averaged power
$\mathcal{P}_i$, $\mathcal{P}_v$ = time-averaged induced and viscous power
$\mathcal{P}_{v0}$ = time-averaged viscous power with zero circulation
$\boldsymbol{Q}$ = vector describing the effect of the drag polar on power
R = propeller radius
Re = Reynolds number
$\mathcal{S}_1$ = time-averaged aerodynamic lateral force
s = distance along airfoil path
T = flapping or rotational period
$\mathcal{T}_1$ = time-averaged thrust
U = flight velocity
V = relative velocity of airfoil through fluid
$\mathcal{V}$ = Trefftz volume
$\boldsymbol{V}$ = vector velocity of fluid
$\boldsymbol{V}_{ij}$ = fluid velocity induced at the ith panel by a unit-strength vortex ring at the jth panel
W = diagonal weighting matrix used in augmented Lagrangian formulation
$\mathcal{W}$ = upper surface of one period of the wake
$\boldsymbol{w}$ = induced wash
x, y, z = Cartesian coordinates
Γ = circulation
$\boldsymbol{\Gamma}$ = vector of potential jumps (circulation) across wake panels
Γ_0 = circulation corresponding to the minimum sectional coefficient of drag
$\Delta\mathcal{A}_j$ = area of the jth vortex-lattice element
Δs_i = length of the ith panel along the airfoil path
Δx_i = extent of the ith element in the x direction
δ_{ij} = Kronecker delta
ζ = coordinate along wingspan
η = propulsive efficiency
θ = amplitude of flapping motion
$\boldsymbol{\lambda}$ = vector of equality constraint Lagrange multipliers
μ = advance ratio; fluid viscosity
ν = inequality constraint Lagrange multiplier
$\boldsymbol{\xi}$ = Kelvin linear impulse
Π = Lagrangian power
Π_a = augmented Lagrangian power
ρ = fluid density
ϕ = velocity potential
Ω = rotational speed of propeller

Subscripts
max = value corresponding to maximum lift condition
R = required value

Presented as Paper 97-0827 at the AIAA 35th Aerospace Sciences Meeting, Reno, NV, Jan. 6–9, 1997; received Feb. 17, 1997; revision received Oct. 21, 1997; accepted for publication Nov. 15, 1997.

*Associate Professor, Department of Mechanical Engineering and Materials Science. Associate Fellow AIAA.
†Graduate Student, Department of Mechanical Engineering and Materials Science.
‡Associate Professor and Raymond L. Bisplinghoff Faculty Fellow, Department of Aeronautics and Astronautics. Associate Fellow AIAA.

I. Introduction

A NUMBER of animals and man-made devices use flapping as a means of producing aerodynamic or hydrodynamic thrust. For example, aircraft and ship propellers flap by rotating, producing a helical wake of trailing vorticity. Helicopter rotors also rotate, but in forward flight produce a skewed wake containing both shed and trailing vorticity. Similarly, birds, bats, and man-made ornithopters generate an undulating wake with both shed and trailing vorticity. For a discussion of the structure of the wakes of birds, bats, and flapping airfoils, see Refs. 1–8. In all of these cases, the wing of the device is made to move with a component of velocity normal to the direction of flight, a condition required to generate thrust. In this paper, we seek to find optimal solutions to the flapping problem. In particular, we present an approach for computing the circulation distribution along a flapping wing that produces a desired aerodynamic force (lift and thrust) with the minimum required power.

A number of investigators have studied the problem of flapping flight by modeling the flowfield induced near the flapping wings as a result of the system of trailing and shed vorticity in the wake. Wilmott[9] developed an unsteady lifting-line theory using the method of matched asymptotic expansions for the general motion of a wing with high aspect ratio. Phlips et al.[10] modeled flapping using an unsteady lifting-line theory in which the shed or transverse vorticity in the wake was lumped at the start of each stroke. Ahmadi and Widnall[11] developed an unsteady lifting-line theory using matched asymptotic expansions, with the inverse of the aspect ratio being the small parameter. Lan[12] developed an unsteady quasi-vortex-lattice method that he then applied to predict the flapping efficiency of various planforms and flapping motions. All of these theories, however, are restricted to low-frequency flapping, i.e., the reduced frequency $k \equiv \Omega b/U << 1$.

None of the preceding analyses address the issue of minimum power flapping flight. The problem of finding the minimum induced loss (MIL) circulation distribution on a flapping wing is conceptually the same as finding the MIL solution for a propeller. The Betz[13] criterion describes the conditions that must be met to obtain an optimum circulation distribution for propellers operating in an inviscid fluid. Goldstein's[14] classic solution for MIL propellers was based on the Betz criterion. Later, Jones[15] applied a similar criterion to solve the problem of thrust generation using low-frequency flapping ($k << 1$) of high aspect ratio wings for the case where the left and right wings flap symmetrically about a common hinge point on the longitudinal axis. Jones was able to find a closed-form solution for the optimum circulation distribution. However, his theory is restricted to low-frequency, small-amplitude flapping motions. Notwithstanding these assumptions, his results predicted that high induced propulsive efficiencies are achieved using flapping motions with large amplitudes and/or high frequencies.

It has been shown that Betz's optimality condition can be generalized to devices other than propellers, such as helicopter rotors (see the Acknowledgments section). Potze and Sparenberg[16] developed a similar optimality criterion for MIL sculling propulsion of ships. Hall et al.,[17] also using a generalized Betz criterion, predicted the optimum circulation distribution for helicopters in forward flight for the case where the rotor must simultaneously generate a prescribed lift, and rolling and pitching moments. More recently, Hall and Hall[18] used this approach to compute the optimum circulation distribution along the span of wings undergoing large-amplitude, high-frequency flapping motion, and generating both lift and thrust. Sparenberg,[19] who has written extensively on optimal hydrodynamic propulsion, also observed that the MIL flapping flight problem could be solved using this approach, although no numerical examples were presented. de Jong[20,21] considered the problem of optimizing the performance of screw propellers, including the effects of viscosity in his analysis. He considered the effect of varying Reynolds number on the viscous drag, but neglected the potential influence of loading, i.e., the dependence of the viscous drag on the lift coefficient as described by the sectional drag polar. de Jong did note that this dependence could be included, if necessary.

In this paper, a method for predicting the minimum power circulation distribution required to generate thrust and lift via the flapping motion of wings is presented. The model extends the method of Hall and Hall[18] by including profile, or viscous, losses. In particular, we allow the sectional coefficient of drag to depend on the sectional lift coefficient. This is especially important for flapping flight because the sectional coefficients of lift and drag vary significantly over the flapping cycle. A variational principle, which is similar in form to the Betz[13] criterion for MIL propellers, describes the optimum circulation distribution in the wake of the flapping wing. A numerical method for solving for the optimality conditions is described. Finally, a number of numerical examples of minimum power circulation distributions for propellers and flapping wings are presented, and the implications of viscous forces on flapping flight are discussed.

II. Theory

A. Lift and Thrust

MIL propeller theory is based on the observation that thrust is a consequence of momentum in the wake, and induced power loss is a consequence of excess kinetic energy in the wake. Therefore, the thrust and power loss can be deduced directly from the structure of the wake, without any reference to how the wake was generated. Likewise, the lift and thrust forces produced in flapping flight are a result of excess momentum deposited in the wake, and the induced power loss is a result of excess kinetic energy deposited in the wake.

The key assumption required in the following development is the light loading assumption. For lightly loaded flapping wings, the induced velocities in the wake are small compared to the velocity of the wings. This implies that the wake sheet left behind the wing will be undistorted by the induced flows, at least for a considerable distance behind the wing. As a result, the far wake will be undistorted and periodic in the flight direction. Hence, the light loading assumption is equivalent to the rigid wake assumption often used in vortex lattice methods.

For the purposes of computing the induced losses arising from wing flapping, we assume that the flow resulting from flapping is inviscid, incompressible, and irrotational (except for the trailing and shed vorticity in the wake). Thus, the three-dimensional flow about the wings and wake is governed by Laplace's equation

$$\nabla^2\phi = 0 \tag{1}$$

where $\boldsymbol{V} = \nabla\phi$. The Cartesian coordinates x, y, and z are taken to be along the longitudinal, lateral, and vertical axes, respectively, as shown in Fig. 1. Furthermore, the coordinates are fixed to the fluid frame of reference so that the velocity of the fluid goes to zero at infinity.

The aerodynamic forces (thrust, side force, and lift) acting on the flapping wing arise when the wing imparts linear momentum to the surrounding fluid. The force averaged over one period of flapping motion is equal and opposite to the time-averaged rate of change in momentum of the flowfield. The

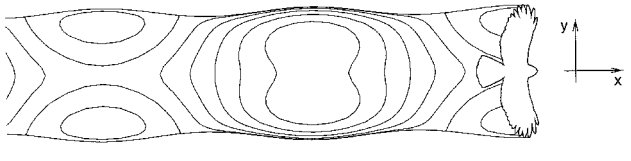

Fig. 1 Top view of bird in flight showing coordinate system and vortex filaments (trailing and shed vorticity) in the wake.

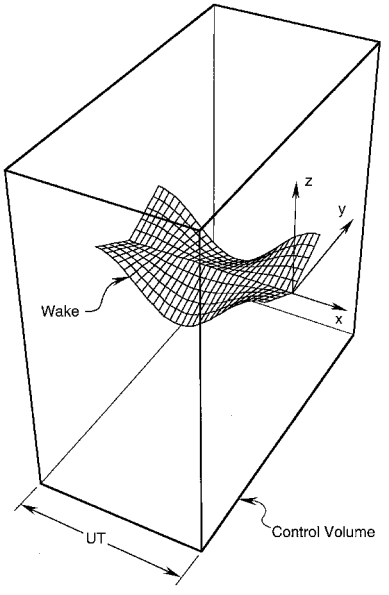

Fig. 2 Control volume enclosing one period of the far wake.

linear momentum $\boldsymbol{\xi}$ deposited in the wake per temporal period T of wing flapping is given by

$$\boldsymbol{\xi} = \rho \int\int\int_{\mathcal{V}} \nabla\phi \, d\mathcal{V} \tag{2}$$

where $T = 2\pi/\Omega$. In Eq. (2), $\mathcal{V}$ is a control volume enclosing one period of the far downstream wake and extending to infinity in the y and z directions (Fig. 2).

Using Gauss' theorem, the volume integral in Eq. (2) may be converted to a surface integral over the surface $\mathcal{A}$ bounding the volume $\mathcal{V}$, so that

$$\boldsymbol{\xi} = -\rho \int\int_{\mathcal{A}} \phi \boldsymbol{n} \, d\mathcal{A} \tag{3}$$

Note that ϕ is periodic in the x direction, and ϕ is continuous, except across the wake. Therefore, ϕ is equal on the upstream and downstream sides of $\mathcal{V}$. Also, the unit normals point in opposite directions on opposite sides of $\mathcal{V}$. Thus, the portion of the integral over the upstream and downstream sides cancel. Finally, ϕ goes to zero exponentially as $|y|$ or $|z|$ goes to infinity. Hence, Eq. (3) reduces to

$$\boldsymbol{\xi} = -\rho \int\int_{\mathcal{S}} \phi \boldsymbol{n} \, d\mathcal{A} \tag{4}$$

where the surface $\mathcal{S}$ includes just the upper and lower sides of the wake.

On either side of the wake, the unit normals $\boldsymbol{n}$ point in opposite directions. Furthermore, the difference in the potentials across the wake is just the bound circulation Γ around the wing at the time the trailing edge of the wing passed by that point in space. Therefore, Eq. (4) can be rewritten as

$$\boldsymbol{\xi} = -\rho \int\int_{W} \Delta\phi \boldsymbol{n} \, d\mathcal{A} = -\rho \int\int_{W} \Gamma \boldsymbol{n} \, d\mathcal{A} \tag{5}$$

Equation (5) may be recognized as the Kelvin linear impulse[22] generated by one period of the wake sheet. The $\boldsymbol{F}$ on the flapping wing is just the negative of the Kelvin linear impulse generated in one wake period, divided by the temporal period T. Therefore,

$$\boldsymbol{F} = -\frac{\boldsymbol{\xi}}{T} = \frac{\rho}{T} \int\int_{W} \Gamma \boldsymbol{n} \, d\mathcal{A} \tag{6}$$

Dotting $\boldsymbol{F}$ with the unit normals $\boldsymbol{i}$, $\boldsymbol{j}$, and $\boldsymbol{k}$ gives the thrust, side force, and lift, respectively, i.e.,

$$\mathcal{T}_1 = \frac{\rho}{T} \int\int_{W} \Gamma \boldsymbol{i} \cdot \boldsymbol{n} \, d\mathcal{A} \tag{7}$$

$$\mathcal{S}_1 = \frac{\rho}{T} \int\int_{W} \Gamma \boldsymbol{j} \cdot \boldsymbol{n} \, d\mathcal{A} \tag{8}$$

$$\mathcal{L}_1 = \frac{\rho}{T} \int\int_{W} \Gamma \boldsymbol{k} \cdot \boldsymbol{n} \, d\mathcal{A} \tag{9}$$

The subscript 1 denotes that these are first-order forces only; induced forces are bookkept as induced power losses, and are considered in the following section.

B. Inviscid-Induced Power

The induced power losses caused by the lift and thrust of a flapping wing arise from the deposition of kinetic energy into the wake. Hence, $\mathcal{P}_i$ is equal to the kinetic energy contained in one period of the wake, divided by the wing-beat period T, so that

$$\mathcal{P}_i = \frac{1}{T} \int\int\int_{\mathcal{V}} \frac{1}{2} \rho |\boldsymbol{V}|^2 \, d\mathcal{V} = \frac{\rho}{2T} \int\int\int_{\mathcal{V}} |\nabla\phi|^2 \, d\mathcal{V} \tag{10}$$

Using the first form of Green's theorem, we have

$$\mathcal{P}_i = \frac{\rho}{2T} \left(-\int\int_{\mathcal{A}} \phi \nabla\phi \cdot \boldsymbol{n} \, d\mathcal{A} - \int\int\int_{\mathcal{V}} \phi \nabla^2\phi \, d\mathcal{V} \right) \tag{11}$$

The second integral in Eq. (11) is identically zero, because $\nabla^2\phi = 0$ in the interior of the volume. The portion of the first integral over the outer surface of $\mathcal{A}$ is also zero, by an argument similar to one used earlier to compute the Kelvin linear impulse. The remainder of the integral is over the upper and lower surface of the wake, so that

$$\mathcal{P}_i = -\frac{\rho}{2T} \int\int_{W} \Delta\phi \nabla\phi \cdot \boldsymbol{n} \, d\mathcal{A} \tag{12}$$

But $\nabla\phi \cdot \boldsymbol{n}$ is equal to $\boldsymbol{w} \cdot \boldsymbol{n}$, the normal wash induced at the surface of the wake, which by continuity must be equal on the upper and lower surface of the wake. Therefore, Eq. (12) may be expressed as

$$\mathcal{P}_i = -\frac{\rho}{2T} \int\int_{W} \Gamma \boldsymbol{w} \cdot \boldsymbol{n} \, d\mathcal{A} \tag{13}$$

Note that $\boldsymbol{w}$ is linearly related to Γ through the Biot–Savart law. Furthermore, the lift and thrust are proportional to the circulation Γ. Thus, the induced power is quadratic in lift and thrust.

C. Viscous Profile Power

Because of the difficulty in computing complex unsteady viscous flows about oscillating airfoils, the simplifying assumption is made that the wing has a large aspect ratio, i.e., $c/b \ll 1$. We further assume that the reduced frequency of flapping based on the airfoil chord is small, so that

$$\Omega c/V \ll 1 \tag{14}$$

where V is given by

$$V = U \frac{ds}{dx} \tag{15}$$

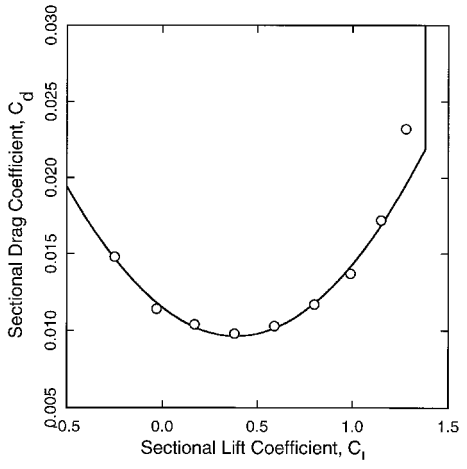

Fig. 3 Two-dimensional drag polar for NACA 4412 airfoil with standard roughness, $Re = 6 \times 10^6$: ○, experimental data[23]; ——, curve fit ($C_{l0} = 0.3863$, $C_{d0} = 0.00964$, $C_{d2} = 0.01242$, $C_{l_{max}} = 1.38$).

and ds/dx is the distance traveled by the wing per unit distance traveled by the wing in the x direction. Under these conditions, the viscous forces may be accurately modeled using quasi-steady lift–drag correlations.

Consider, for example, the drag polar shown in Fig. 3 for a NACA 4412 airfoil with standard surface roughness operating at $Re = 6 \times 10^6$, where $Re \equiv \rho Vc/\mu$. Shown is the experimentally measured coefficient of C_d as a function of the coefficient of C_l for steady flow as reported by Abbott, et al.[23] where

$$C_l \equiv \frac{l}{\frac{1}{2}\rho V^2 c} \quad \text{and} \quad C_d \equiv \frac{d}{\frac{1}{2}\rho V^2 c} \tag{16}$$

For moderate to large Reynolds numbers, the sectional drag is predominantly a function of the sectional lift, and only weakly dependent on the Reynolds number. Also, for angles of attack away from stall, the drag can generally be approximated as a quadratic function of the lift, so that

$$C_d \approx C_{d0} + C_{d2}(C_l - C_{l0})^2 \tag{17}$$

where C_{d0}, C_{d2}, and C_{l0} are constants that depend on the particular airfoil profile and Reynolds number. For the present example of a NACA 4412 airfoil, $C_{l0} = 0.3863$, $C_{d0} = 0.00964$, and $C_{d2} = 0.01242$. This correlation is plotted in Fig. 3 and is seen to be in good agreement with the experimental data over a wide range of sectional lift coefficients.

For large angles of attack, the airfoil will stall, and the correlation given by Eq. (17) will fail. Physically, such situations are to be avoided because they result in large viscous power losses with little or no additional thrust production. Thus, a constraint is imposed so that the flapping motion is

$$\Gamma \leq \Gamma_{\max} \tag{18}$$

The coefficient of lift C_l may be expressed in terms of the circulation as

$$C_l = \frac{l}{\frac{1}{2}\rho V^2 c} = \frac{2\Gamma}{Vc} \tag{19}$$

Hence, $\Gamma_{\max} = \frac{1}{2} Vc C_{l_{\max}}$, with $C_{l_{\max}}$ taken here to be 1.38.

The profile power $\mathcal{P}_v$ resulting from flapping may be expressed as the work per cycle divided by the period, so that

$$\mathcal{P}_v = \frac{1}{T} \int \int_W \frac{1}{2} \rho V^2 c C_d \, d\mathcal{A} \tag{20}$$

Substitution of Eqs. (15–17) and Eq. (19) into Eq. (20) gives

$$\mathcal{P}_v = \frac{\rho}{2T} \int \int_W (U^2 c C_{d0}) \cdot \left(\frac{ds}{dx}\right)^2 d\mathcal{A} + \frac{\rho}{2T} \int \int_W \left(\frac{4C_{d2}}{c}\right) \cdot (\Gamma - \Gamma_0)^2 \, d\mathcal{A} \tag{21}$$

Finally, the total power loss $\mathcal{P}$, which is the sum of the induced and profile powers, is given by

$$\mathcal{P} = \mathcal{P}_i + \mathcal{P}_v = -\frac{\rho}{2T} \int \int_W \Gamma \boldsymbol{w} \cdot \boldsymbol{n} \, d\mathcal{A} + \frac{\rho}{2T} \int \int_W \left(\frac{4C_{d2}}{c}\right) (\Gamma - \Gamma_0)^2 \, d\mathcal{A} + \frac{\rho}{2T} \int \int_W (U^2 c C_{d0}) \cdot \left(\frac{ds}{dx}\right)^2 d\mathcal{A} \tag{22}$$

Note that the total power loss may be expressed in terms of the shape of the wake, the planform of the wing, the quasi-steady sectional drag polar, and the circulation distribution in the wake. For a given wing undergoing a prescribed flapping motion, only the circulation is unknown. Furthermore, the profile power is quadratic in the circulation Γ, a fact that will prove useful when computing the optimum circulation distribution.

D. Optimal Solution to the Large-Amplitude Flapping Problem

To find the circulation that minimizes the total power loss in the prescribed flight condition, the constraints are adjoined to the power using Lagrange multipliers $\boldsymbol{\lambda}$ and ν to form the Lagrangian power

$$\Pi = \mathcal{P} + \boldsymbol{\lambda} \cdot (\boldsymbol{F} - \boldsymbol{F}_R) + \frac{\rho}{T} \int \int_W \nu (\Gamma - \Gamma_{\max}) \, d\mathcal{A} \tag{23}$$

The ν is zero if the inequality constraint [Eq. (18)] is inactive, and positive if it is active. Taking the variation of Eq. (23), one obtains

$$\delta\Pi = \delta\boldsymbol{\lambda} \cdot (\boldsymbol{F} - \boldsymbol{F}_R) + \frac{\rho}{T} \int \int_W \delta\nu (\Gamma - \Gamma_{\max}) \, d\mathcal{A} + \frac{\rho}{T} \int \int_W \left[\boldsymbol{\lambda} \cdot \boldsymbol{n} - \boldsymbol{w} \cdot \boldsymbol{n} + \frac{4C_{d2}}{c} (\Gamma - \Gamma_0) + \nu\right] \delta\Gamma \, d\mathcal{A} \tag{24}$$

where we have used the potential flow identity

$$\int \int_W \boldsymbol{w} \cdot \boldsymbol{n} \delta\Gamma \, d\mathcal{A} = \int \int_W \delta\boldsymbol{w} \cdot \boldsymbol{n} \Gamma \, d\mathcal{A} \tag{25}$$

to eliminate $\delta\boldsymbol{w}$ from the integrand of the second integral in Eq. (24). At the constrained optimum, Π is stationary ($\delta\Pi = 0$). Therefore, the necessary conditions for minimum power are

$$\mathcal{T}_1 = \mathcal{T}_R \tag{26}$$

$$\mathcal{S}_1 = \mathcal{S}_R \tag{27}$$

$$\mathcal{L}_1 = \mathcal{L}_R \tag{28}$$

$$\nu \geq 0 \quad \text{if} \quad \Gamma = \Gamma_{\max}$$
$$\nu = 0 \quad \text{if} \quad \Gamma < \Gamma_{\max} \tag{29}$$

and finally

$$\boldsymbol{w}\cdot\boldsymbol{n} = \boldsymbol{\lambda}\cdot\boldsymbol{n} + (4C_{d2}/c)(\Gamma - \Gamma_0) + \nu \tag{30}$$

Equation (30) is the viscous equivalent of the Betz[13] criterion. The physical interpretation of Eq. (30), at least for cases when the inequality constraint is inactive ($\nu = 0$), is that the optimum-induced normal wash on the wake is equal to the normal wash induced at the surface of the wake by an impermeable surface (the wake sheet) translating with velocity $\boldsymbol{\lambda}$, plus a term proportional to the coefficient C_{d2} times the deviation of Γ away from Γ_0. Note in particular that because C_{d0} has no effect on the first-order thrust or lift, and is not a function of Γ, it has no influence on the optimum distribution of circulation along the wake. Furthermore, the coefficient C_{d2} is usually small, typically $\mathcal{O}(10^{-2})$. Thus, at least for lightly loaded cases, the optimum viscous circulation distribution is nearly equal to the optimum inviscid distribution. Of course, the total power loss $\mathcal{P}$ is increased by the presence of viscous forces, even if the optimum circulation distribution is not significantly different from the inviscid case.

If the inequality constraint is active, then the preceding interpretation of the optimality conditions is slightly modified. In regions of the wake where $\Gamma < \Gamma_{\max}$, the optimal induced wash at the wake is as described earlier. In regions where $\Gamma = \Gamma_{\max}$, however, the induced normal wash (which is usually negative), is increased by ν, i.e., the magnitude of the normal wash is usually reduced.

III. Numerical Solution Technique

In Sec. II, a variational principle for the optimum circulation distribution in flapping flight was developed. In this section, a technique for discretizing and solving the variational principle is described.

To calculate these integral quantities, a vortex-lattice model is used. One period of the wake (the reference period) is divided into N quadrilateral elements. Each element is bounded by a vortex filament of strength Γ_j. Thus, the potential jump across the jth element is just Γ_j, and the time-averaged force on the flapping wing may be approximated by

$$\boldsymbol{F} = \begin{Bmatrix} \mathcal{T}_1 \\ \mathcal{S}_1 \\ \mathcal{L}_1 \end{Bmatrix} = \sum_{j=1}^{N} \boldsymbol{b}_j \Gamma_j = B\boldsymbol{\Gamma} \tag{31}$$

where

$$\boldsymbol{b}_j = (\rho/T)\boldsymbol{n}_j \Delta\mathcal{A}_j \tag{32}$$

and $\boldsymbol{\Gamma}$ is a vector whose jth entry is just Γ_j. The unit normal at the center of the jth element is $\boldsymbol{n}_j$, and $\Delta\mathcal{A}_j$ is the area of the element.

Likewise, the power is approximated by

$$\mathcal{P} = \frac{1}{2}\sum_{i=1}^{N}\sum_{j=1}^{N} K_{ij}\Gamma_i\Gamma_j - \sum_{i=1}^{N} Q_i\Gamma_i + \mathcal{P}_{v0}$$

$$= \frac{1}{2}\boldsymbol{\Gamma}^T K\boldsymbol{\Gamma} - \boldsymbol{\Gamma}^T\boldsymbol{Q} + \mathcal{P}_{v0} \tag{33}$$

with

$$K_{ij} = -\frac{\rho}{T}\boldsymbol{V}_{ij}\cdot\boldsymbol{n}_i\Delta\mathcal{A}_i + \delta_{ij}\frac{\rho}{T}\frac{4C_{d2}}{c_i}\Delta\mathcal{A}_i \tag{34}$$

$$Q_i = \frac{\rho}{T}\frac{4C_{d2}}{c_i}\Gamma_{0i}\Delta\mathcal{A}_i \tag{35}$$

$$\mathcal{P}_{v0} = \frac{\rho}{2T}\sum_{i=1}^{N} U^2[c(C_{d0} + C_{d2}C_{l0}^2)]_i\cdot\left(\frac{\Delta s_i}{\Delta x_i}\right)^2\Delta\mathcal{A}_i \tag{36}$$

In Eq. (34), $\boldsymbol{V}_{ij}$ is the velocity at the center of the ith panel induced by an infinite row of vortex ring panels of unit strength spaced a distance UT apart in the x direction, with the reference sending panel located at the jth position in the grid. Standard numerical techniques are used to compute the induced wash. For panels that are close to the collocation point, the exact wash caused by a quadrilateral vortex ring is computed.[24] For panels that are far from the collocation point, the vortex ring panel is approximated by a point doublet oriented in the direction normal to the panel surface. This approximation reduces the computational time required to assemble the influence coefficients $\boldsymbol{V}_{ij}$.

For the case where the maximum coefficient of lift constraint is inactive, the Lagrangian power may be expressed in matrix form as

$$\Pi = \frac{1}{2}\boldsymbol{\Gamma}^T K\boldsymbol{\Gamma} - \boldsymbol{\Gamma}^T\boldsymbol{Q} + \boldsymbol{\lambda}^T(B\boldsymbol{\Gamma} - \boldsymbol{F}_R) + \mathcal{P}_{v0} \tag{37}$$

Taking the variation of Eq. (37) and setting the result to zero gives the desired set of linear equations that describe the optimum solution, i.e.,

$$\begin{bmatrix} K & B^T \\ B & 0 \end{bmatrix}\begin{Bmatrix} \boldsymbol{\Gamma} \\ \boldsymbol{\lambda} \end{Bmatrix} = \begin{Bmatrix} \boldsymbol{Q} \\ \boldsymbol{F}_R \end{Bmatrix} \tag{38}$$

Equation (38) is solved using Gaussian elimination for the unknown circulation distribution $\boldsymbol{\Gamma}$ and Lagrange multiplier $\boldsymbol{\lambda}$.

If after solving Eq. (38) it is found that the maximum coefficient of lift constraint is violated at any point along the wake, additional steps are required to compute the constrained optimum. Because the maximum coefficient of lift constraint is nonlinear, it cannot be added to Eq. (38) in the same (linear) way as the thrust constraint. Instead, we use the method of mathematical programming via augmented Lagrangians.[17,25] The procedure is as follows. At the points along the wake where the maximum coefficient of lift is violated, the constraint is activated. A quadratic penalty function is added to the Lagrangian power that increases the power when the constraint is violated. Thus, Π_a is expressed as

$$\Pi_a = \tfrac{1}{2}\boldsymbol{\Gamma}^T K\boldsymbol{\Gamma} - \boldsymbol{\Gamma}^T\boldsymbol{Q} + \boldsymbol{\lambda}^T(B\boldsymbol{\Gamma} - \boldsymbol{F}_R) + \boldsymbol{\nu}^T(\boldsymbol{\Gamma} - \boldsymbol{\Gamma}_{\max}) + \tfrac{1}{2}(\boldsymbol{\Gamma} - \boldsymbol{\Gamma}_{\max})^T W(\boldsymbol{\Gamma} - \boldsymbol{\Gamma}_{\max}) + \mathcal{P}_{v0} \tag{39}$$

where W is a diagonal matrix with large positive entries corresponding to the active constraints with zero diagonal entries elsewhere, and $\boldsymbol{\nu}$ is the vector of inequality constraint Lagrange multipliers. Taking the variation of Eq. (39) and setting the result to zero yields

$$\begin{bmatrix} K + W & B^T \\ B & 0 \end{bmatrix}\begin{Bmatrix} \boldsymbol{\Gamma} \\ \boldsymbol{\lambda} \end{Bmatrix} = \begin{Bmatrix} \boldsymbol{Q} + W\boldsymbol{\Gamma}_{\max} - \boldsymbol{\nu} \\ \boldsymbol{F}_R \end{Bmatrix} \tag{40}$$

Equation (40) is solved using Gaussian elimination.

Examining Eq. (40), it can be seen that for large W, active constraints will be very nearly satisfied. Furthermore, the term $\boldsymbol{\nu} + W(\boldsymbol{\Gamma} - \boldsymbol{\Gamma}_{\max})$ plays the role of the inequality constraint Lagrange multiplier. Thus, an improved estimate of the Lagrange multiplier is given by

$$\boldsymbol{\nu}_{\text{new}} = \boldsymbol{\nu}_{\text{old}} + W(\boldsymbol{\Gamma} - \boldsymbol{\Gamma}_{\max}) \tag{41}$$

Having obtained an improved estimate of the solution, the constraint list is updated. If the new estimate of a particular Lagrange multiplier is positive, then the constraint is kept active. If the Lagrange multiplier is negative, then the constraint should be inactive. Thus, the Lagrange multiplier is set to zero and the corresponding diagonal entry in the W matrix is set to zero. On the other hand, if a previously inactive constraint is violated after the solution of Eq. (40), then that constraint is

made active by setting the corresponding diagonal entry in W to a large positive value. The process is repeated [Eqs. (40) and (41) and the constraint checks] until a converged solution is achieved. Typically, fewer than five iterations are required to obtain a converged solution.

Finally, the computed circulation can then be substituted into Eq. (33) to obtain the minimum excess power required to generate thrust in a viscous fluid.

IV. Results

In this section, the method described in Sec. III is used to compute the optimal circulation distribution for two different geometries. In Sec. IV.A, a two-bladed propeller is considered. In essence, a propeller generates thrust using rotational flapping rather than reciprocal flapping about the longitudinal axis as in the case of flying animals or ornithopters. The case of a propeller is useful because Goldstein[14] has found solutions to the minimum induced loss problem for propellers operating at small advance ratios, a condition equivalent to large-amplitude, high-frequency flapping. In Sec. IV.B, the case of a flapping wing in forward flight that must simultaneously generate thrust and lift is considered.

A. Two-Bladed Propeller

To test the accuracy of the present method, we first use the method to compute the minimum induced power circulation distribution for a two-bladed propeller with radius R, rotating with speed Ω, with forward velocity U, and generating thrust $\mathcal{T}_1$. Furthermore, c is taken to be constant over the span of the blade and equal to $R/6$. The airfoil section used is a NACA 4412 airfoil with drag polar as in Fig. 3. Figure 4 shows the computed minimum induced power loss distribution for a propeller operating at two different advance ratios, $\mu = 0.1$ and 0.5, where

$$\mu \equiv U/\Omega R \tag{42}$$

These solutions were computed using a vortex-lattice mesh with 32×32 vortex ring elements per turn of the wake. Also shown for comparison are the analytical results tabulated by Goldstein.[14] Note that the present method is in almost exact agreement with Goldstein's classical solution. Note, however, that these solutions only account for induced losses.

Next, the optimal viscous circulation distribution was computed for the case where the propeller operates at an advance ratio μ of 0.45 (nondimensional rotational frequency $k \equiv 1/\mu = 2.22$) for two different thrust coefficients, $C_{\mathcal{T}_1} = 0.4$ and $C_{\mathcal{T}_1} = 0.8$, where

$$C_{\mathcal{T}_1} \equiv \frac{\mathcal{T}_1}{\frac{1}{2}\rho U^2 R^2} \quad \text{and} \quad C_{\mathcal{P}} \equiv \frac{\mathcal{P}}{\frac{1}{2}\rho U^3 R^2} \tag{43}$$

The computed solutions are shown in Fig. 5. These and subsequent propeller solutions were computed using a vortex-lattice mesh with 25×32 vortex ring elements per turn of the wake. Also shown for comparison is the optimal inviscid solution. Note that for the more lightly loaded case, $C_{\mathcal{T}_1} = 0.4$, the optimal inviscid and viscous circulation distributions are very similar. In the viscous case, the loading is shifted very slightly towards the tips. This reduces the large profile drag associated with large sectional lift coefficients on the inboard portion of the propeller where the relative velocity is small. At the higher loading condition, $C_{\mathcal{T}_1} = 0.8$, the maximum coefficient of lift constraint is active over a large portion of the blade, reducing the circulation. Thus, the circulation must be increased near the tip to obtain the desired thrust. The results shown in Fig. 5 are typical; if the maximum coefficient of lift constraint is not active then viscous effects have only a small influence on the optimal circulation distribution.

Next, we computed the power loss for this propeller for several different nondimensional rotational frequencies, $1/\mu$.

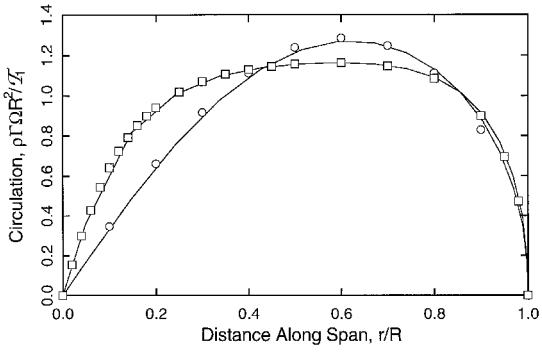

Fig. 4 Optimum circulation distribution for inviscid two-bladed propeller at two different advance ratios. ——, present vortex-lattice method; □, Goldstein[14] theory with advance ratio $\mu = 0.1$; 0, $\mu = 0.5$.

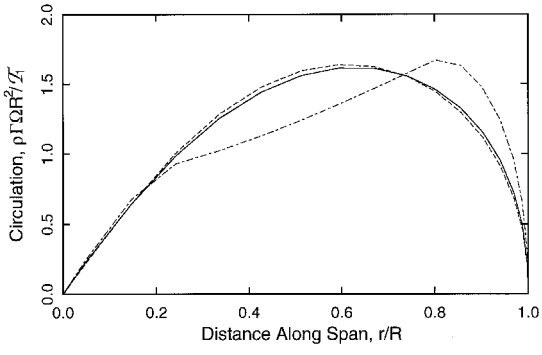

Fig. 5 Optimum circulation distribution for two-bladed propeller with $\mu = 0.45$. – –, inviscid; ——, viscous with $C_{\mathcal{T}_1} = 0.4$; – – – –, viscous with $C_{\mathcal{T}_1} = 0.8$.

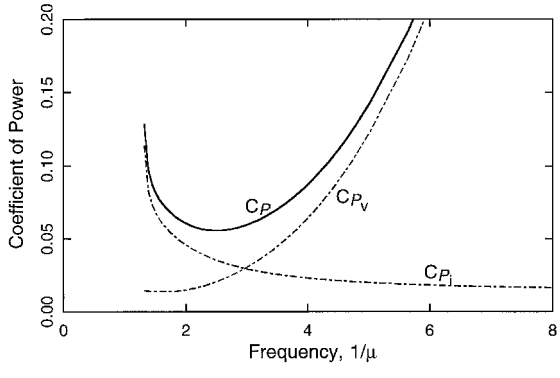

Fig. 6 Power loss for optimally loaded propeller at various rotational speeds, $C_{\mathcal{T}_1} = 0.4$.

Shown in Fig. 6 is the power loss as a function of rotation speed for an optimally loaded viscous propeller with thrust coefficient $C_{\mathcal{T}_1} = 0.4$. The total power loss is the sum of the induced (inviscid) and profile (viscous) losses. The induced losses are seen to decrease with increasing rotational frequency until the actuator disk limit of efficiency is reached, $C_{\mathcal{P}_i} \sim C_{\mathcal{T}_1}^2/4\pi$. Profile losses, on the other hand, generally increase with increasing rotational speed, although there can be a modest rise in viscous losses at very low rotational speeds caused by large local sectional coefficients of lift. Thus, the optimal rotation frequency is at an intermediate frequency, in this case $1/\mu \approx 2.5$. At this frequency, the propulsive efficiency, defined here as

$$\eta \equiv \frac{C_{\mathcal{T}_1}}{C_{\mathcal{T}_1} + C_{\mathcal{P}}} \tag{44}$$

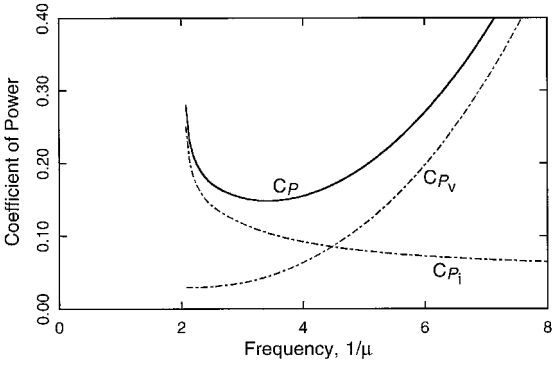

Fig. 7 Power loss for optimally loaded propeller at various rotational speeds, $C_{\mathcal{T}_1} = 0.8$.

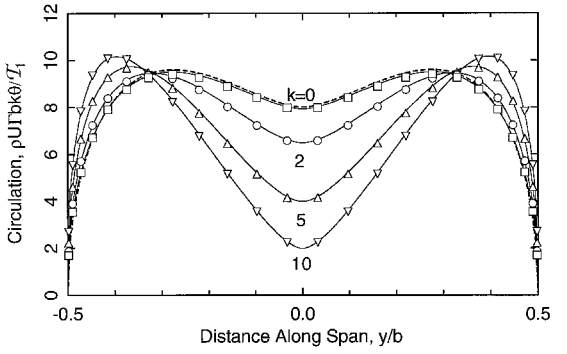

Fig. 8 Minimum induced power circulation distributions for thrust caused by flapping: ——, small-amplitude harmonic theory of Hall and Hall[18]; – – –, Jones' theory[15]; □, ○, △, and , present method with θ = 1 deg.

is equal to 0.878. Also note that the power loss rises sharply at low rotational frequencies. For frequencies $1/\mu$ less than about 1.3, no feasible solution exists, that is, the propeller is stalled over the entire span.

Next, we consider the same propeller, but this time operating at a thrust coefficient $C_{\mathcal{T}_1} = 0.8$. The computed power loss is shown in Fig. 7. Note that, as expected, the power loss is somewhat larger than in the previous example because the induced loss scales with the square of the thrust. The profile losses, on the other hand, do not change substantially. Thus, because the induced losses are relatively more important, the optimal rotation frequency of the propeller is somewhat larger than in the previous example with $1/\mu \approx 3.4$. At this frequency, η is about 0.875.

Note that in the examples presented in Figs. 6 and 7, the local pitch of the blade is adjusted at every rotation speed to obtain the optimum circulation distribution. In real propellers, of course, pitch cannot be varied along the span of the blade. Thus, the minimum power loss curves shown in these figures should be considered lower bounds of the power loss for a fixed-pitch propeller of a given planform.

B. Flapping of a Rigid Wing

In this section, we compute the optimal circulation distributions and corresponding power requirements for a wing in flapping flight. The wing is assumed to have a rectangular planform with span b and an aspect ratio of 6.0. As in the previous propeller example, the airfoil section is a NACA 4412 airfoil with drag polar as in Fig. 3. We consider flapping motions where the wake has the following shape:

$$\left.\begin{aligned} z &= |\zeta|\sin[\theta\cos(\Omega x/U)] \\ y &= |\zeta|\cos[\theta\cos(\Omega x/U)] \end{aligned}\right\} \quad \text{for} \quad |\zeta| \le b/2 \tag{45}$$

where Ω is the flapping frequency, and θ is the angular amplitude of flapping motion. This motion corresponds to a wing with a straight, unswept trailing edge flapping rigidly about a hinge point on the longitudinal axis.

For the first example, the amplitude of flapping is small with $\theta = 1$ deg, and only induced losses are considered. Shown in Fig. 8 is the optimum circulation required to produce thrust with no lift. The circulation is plotted at the point in the downstroke when the wings pass through the horizontal position. These and subsequent results were computed using a vortex-lattice mesh with 24 elements per period in the flight direction, and 24 elements in the spanwise direction. Each solution required about 18 s of CPU time to compute on a Silicon Graphics Inc. (SGI) Power Indigo^2 workstation. Also shown is Jones'[15] exact solution to the optimal circulation problem for low-frequency small-amplitude flapping, and the small-amplitude harmonic theory developed by Hall and Hall.[18] The present method is seen to be in excellent agreement with the other two theories, at least for this small-amplitude case.

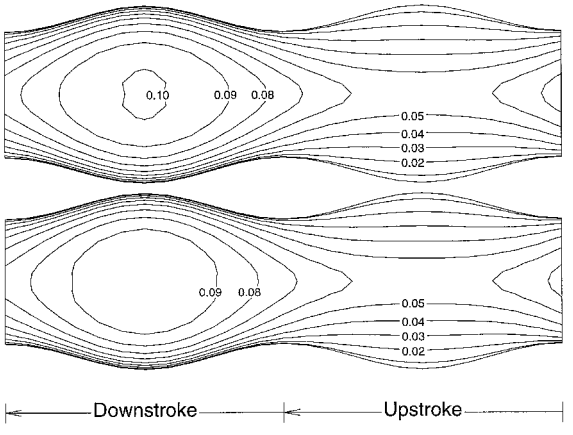

Fig. 9 Top view of optimal circulation distribution in wake of flapping wing. θ = 45 deg, μ = 0.5, $C_{\mathcal{L}_1} = 0.1$, $C_{\mathcal{T}_1} = 0.01$. Top: inviscid solution; bottom: viscous solution. Direction of flight is right to left. Plotted are contours of Γ/Ub.

Next, we consider the case of large-amplitude flapping where the flapping wing must simultaneously generate both thrust and lift. Shown in Fig. 9 is the optimal circulation distribution in the wake of a flapping wing with $1/\mu = 2.0$, $\theta = 45$ deg, $C_{\mathcal{L}_1} = 0.1$, and $C_{\mathcal{T}_1} = 0.01$, where

$$k \equiv \frac{1}{\mu} \equiv \frac{\Omega b}{U} \tag{46}$$

$$C_{\mathcal{L}_1} \equiv \frac{\mathcal{L}_1}{\frac{1}{2}\rho U^2 b^2}, \qquad C_{\mathcal{T}_1} \equiv \frac{\mathcal{T}_1}{\frac{1}{2}\rho U^2 b^2}, \qquad C_{\mathcal{P}} \equiv \frac{\mathcal{P}}{\frac{1}{2}\rho U^3 b^2} \tag{47}$$

Two cases are shown, one in which the optimal circulation distribution is computed considering only induced losses, and the other with profile losses included. The two solutions are very similar, with the largest differences occurring at the middle of the wake during the downstroke. One sees that the inviscid circulation is very slightly larger in this region. In the viscous solution, the circulation is reduced slightly in this region to minimize the profile losses associated with large sectional lift coefficients.

Figure 10 shows the optimal circulation distribution for the same case shown in Fig. 9, but with the thrust coefficient $C_{\mathcal{T}_1}$ now increased to 0.2. Over a portion of the downstroke, the maximum coefficient of sectional lift constraint is active over the inboard portion of the wing, reducing the circulation in this region. Also note that over a portion of the upstroke, the circulation near the tips is negative.

Next, the power losses were computed for the flapping wing. Figure 11 shows the power loss for an optimally loaded flap-

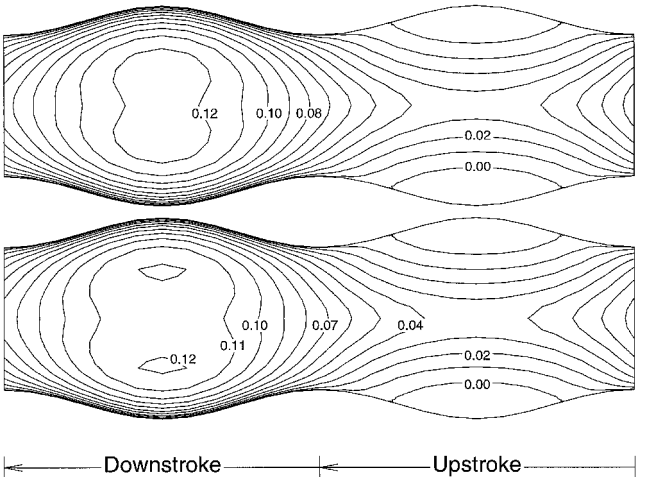

Fig. 10 Top view of optimal circulation distribution in wake of flapping wing. θ = 45 deg, μ = 0.5, $C_{\mathcal{L}_1}$ = 0.1, $C_{\mathcal{T}_1}$ = 0.02. Top: inviscid solution; bottom: viscous solution.

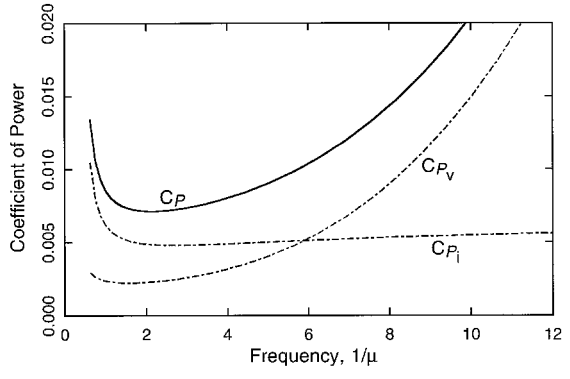

Fig. 11 Power loss for optimally loaded flapping wing at various flapping frequencies. θ = 45 deg, $C_{\mathcal{L}_1}$ = 0.1, $C_{\mathcal{T}_1}$ = 0.01.

ping wing for a range of flapping frequencies 1/μ for the case where θ = 45 deg, $C_{\mathcal{L}_1}$ = 0.1, and $C_{\mathcal{T}_1}$ = 0.01. Note the striking similarity of these results to those of a propeller (see Figs. 6 and 7). Again, the induced losses generally decrease with increasing flapping frequency, whereas the profile losses generally increase. One notable difference is that the induced losses become relatively flat at moderate reduced frequencies, and may even increase slightly for very large frequencies. This is because, unlike a propeller, a flapping wing must generate both thrust and lift. While the (inviscid) generation of thrust becomes more efficient at large flapping frequencies, approaching the actuator disk limit, the generation of lift is most efficient at low frequencies. For this example, the optimal flapping frequency 1/μ is approximately 2.1.

For a propeller, which has the sole purpose of generating thrust, the propulsive efficiency is simply the thrust power produced divided by the total power (thrust power plus power losses). For a flapping wing, which must produce both thrust and power, we may define the propulsive efficiency as

$$\eta \equiv \frac{C_{\mathcal{T}_1}}{C_{\mathcal{T}_1} + C_{\mathcal{P}} - C_{\mathcal{P}_0}} \tag{48}$$

where $C_{\mathcal{P}_0}$ is the power loss with θ = 0, $C_{\mathcal{T}_1}$ = 0, and $C_{\mathcal{L}_1}$ = 0.1. In other words, only the increase in power required to generate thrust should be counted in the calculation of efficiency. Using this definition, we find that the propulsive efficiency of the flapping wing discussed in the previous example is approximately equal to 0.808 at a flapping frequency 1/μ of 2.1.

Figure 12 shows the optimal power loss for the same case presented in Fig. 11, but with $C_{\mathcal{T}_1}$ = 0.02. For this more highly loaded case, the optimal flapping frequency 1/μ is about 3.1, and the corresponding η is 0.837.

In the previous two examples, the minimum power loss for flapping flight was computed for two different thrust coefficients. The flapping amplitude was fixed (θ = 45 deg) and the flapping frequency 1/μ was varied. Next, we consider the effect of flapping amplitude on power losses. Shown in Figs. 13 and 14 are contours of power loss $C_{\mathcal{P}}$ as a function of flapping

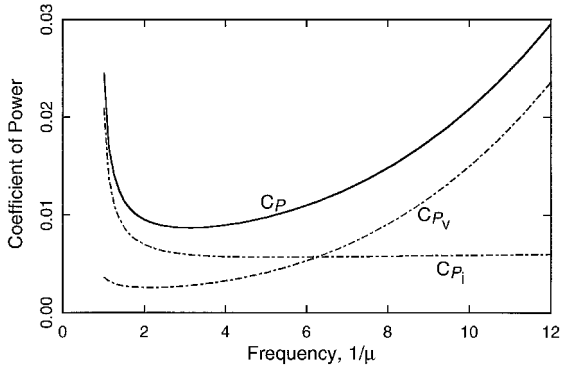

Fig. 12 Power loss for optimally loaded flapping wing at various flapping frequencies. θ = 45 deg, $C_{\mathcal{L}_1}$ = 0.1, $C_{\mathcal{T}_1}$ = 0.02.

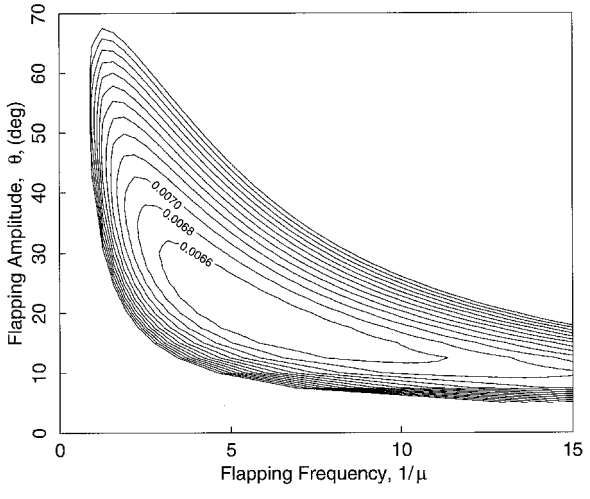

Fig. 13 Power loss $C_{\mathcal{P}}$ for various flapping amplitudes and frequencies, $C_{\mathcal{L}_1}$ = 0.1, $C_{\mathcal{T}_1}$ = 0.01.

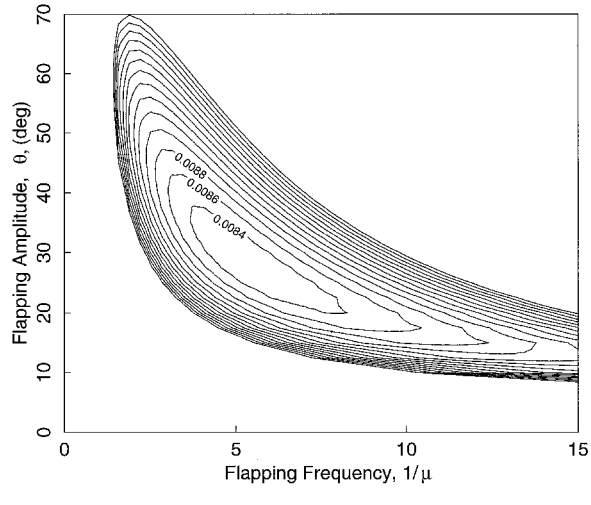

Fig. 14 Power loss $C_{\mathcal{P}}$ for various flapping amplitudes and frequencies, $C_{\mathcal{L}_1}$ = 0.1, $C_{\mathcal{T}_1}$ = 0.02.

frequency and amplitude for two different thrust coefficients, $C_{\mathcal{T}_1} = 0.01$ and 0.02. Note that for each case, there is an optimum amplitude and frequency that produces the minimum power loss. For the lower thrust loading case, $C_{\mathcal{T}_1} = 0.01$, the minimum power $C_{\mathcal{P}}$ is about 0.00641, corresponding to $\theta = 20$ deg and $1/\mu = 5.3$. Under these conditions, η is approximately 0.859. This flapping frequency corresponds to slightly less than one wing beat per wingspan traveled. For the higher thrust loading case, $C_{\mathcal{T}_1} = 0.02$, the minimum power $C_{\mathcal{P}}$ is approximately 0.00825, corresponding to $\theta = 27$ deg and $1/\mu = 5.3$. The corresponding η is about 0.852. Thus, flapping flight is seen to be remarkably efficient, with propulsive efficiencies rivaling that of propellers. Note that the optimum flapping frequency is relatively insensitive to thrust loading. The optimum flapping amplitude, however, is sensitive to thrust loading.

V. Summary and Discussion

A variational method has been developed for computing the minimum power circulation distribution along the span of a flapping wing that must simultaneously generate thrust and lift. Using this approach, the sum of the induced (inviscid) power and profile (viscous) power are minimized subject to the constraints that the desired thrust and lift be obtained and that no portion of the wing may operate in a stalled condition. The resulting variational statement is the viscous equivalent of the well-known Betz criterion for MIL propellers. This variational principle is solved numerically using a vortex-lattice method to compute the lift, thrust, and induced power and a quasi-steady drag polar correlation to model profile drag. Inequality constraints are implemented using an augmented Lagrangian method. The present method is computationally very efficient. For cases in which the maximum sectional coefficient of lift constraint is active, the analysis typically requires less than 2 min of CPU time on an SGI Power Indigo^2. For lightly loaded cases in which the constraint is inactive, solutions require about 18 s of computer time.

The method was used to compute minimum induced power loss circulation distributions of a propeller and a flapping wing. For the case of inviscid propellers, the present method was found to predict circulation distributions that are in good agreement with Goldstein's[14] classic MIL propeller theory. For the case of small-amplitude wing flapping, the present theory also recovers the minimum induced circulation distribution predicted by Jones,[15] and the small-amplitude flapping theory of Hall and Hall.[18]

The method was also used to compute optimal circulation distributions for propellers and flapping wings operating in a viscous fluid. One interesting result is that the optimal viscous circulation distribution is very nearly equal to the optimal inviscid circulation distribution, provided that the maximum coefficient of lift constraint is not active. For typical levels of required thrust, the optimal propulsive efficiency of a constant chord propeller was found to be about 0.88 at a rotational frequency that increases with thrust. For a flapping wing that must generate both thrust and lift, the situation is similar. The optimal propulsive efficiency was found to be about 0.85 for two different thrust levels. The optimal flapping frequency $1/\mu$ was found to about 5.3, and relatively insensitive to thrust requirements. This flapping frequency means that the wing should flap slightly less than once for every one wingspan the wing flies forward through the air.

The present theory accounts for aerodynamic effects only. Mechanical and physiological losses are not considered. In birds, it may be desirable for physiological reasons for the bird to flap its wings at frequencies lower than the aerodynamically optimal frequency. In fact, birds in fast forward flight are observed to flap their wings over a range of moderately large reduced nondimensional frequencies. For example, Tucker[26,27] studied the flight of budgerigars (*Melopsittacus undulatus*) in a wind tunnel. He observed that one specimen with a b of 0.235 m flapped its wings with a constant beat frequency Ω of 88 rad s^{-1} for a range of flight speeds U from 5.3 m to 13.3 m s^{-1}. This corresponds to a range of k from 1.55 to 3.90. Similarly, Tucker[27,28] measured the flapping frequency of a laughing gull (*Larus atricilla*) with a b of 0.93 m to be a constant 23.8 rad s^{-1} over a range of flight speeds from 8.6 to 11.2 m s^{-1} corresponding to k between 1.98 and 2.57. Fortunately, the minimum power solution (Figs. 13 and 14) has a trough or valley of low power. Thus, the wings may be flapped at a lower than optimum frequency with little increase in power if the flapping amplitude is appropriately raised.

Acknowledgments

The authors acknowledge the useful but unpublished report on "The Theory of the Lightly-Loaded Propeller," by D. Munro, written in 1979 when he was a graduate student in the Department of Aeronautics and Astronautics at the Massachusetts Institute of Technology. In particular, he pointed out the possibility of extending Betz's optimality condition to the case of a helicopter rotor in forward flight. In addition, the authors thank J. A. Sparenberg for pointing out connections between optimum hydrodynamic propulsion and our research.

References

[1]Rayner, J. M. V., "Wake Structure and Force Generation in Avian Flapping Flight," *Acta XX Congressus Internationalis Ornithologici*, edited by B. D. Bell, Ornithological Congress Trust Board, Wellington, New Zealand, Vol. 2, 1991, pp. 702–715.

[2]Rayner, J. M. V., "A Vortex Theory of Animal Flight. Part 2. The Forward Flight of Birds," *Journal of Fluid Mechanics*, Vol. 91, Pt. 4, 1979, pp. 731–763.

[3]Rayner, J. M. V., "On Aerodynamics and the Energetics of Vertebrate Flapping Flight," *Fluid Dynamics in Biology*, edited by A. Y. Cheer and C. P. van Dam, Vol. 141, Contemporary Mathematics, American Mathematical Society, Providence, RI, 1993, pp. 351–400.

[4]Rayner, J. M. V., Jones, G., and Thomas, A., "Vortex Flow Visualizations Reveal Change in Upstroke Function with Flight Speed in Bats," *Nature*, Vol. 321, May 1986, pp. 162–164.

[5]Spedding, G. R., "The Wake of a Jackdaw (*Corvus monedula*) in Slow Flight," *Journal of Experimental Biology*, Vol. 125, Sept. 1986, pp. 287–307.

[6]Spedding, G. R., "The Wake of a Kestrel (*Falco tinnunculus*) in Flapping Flight," *Journal of Experimental Biology*, Vol. 127, Jan. 1987, pp. 59–78.

[7]Spedding, G. R., Rayner, J. M. V., and Pennycuick, C. J., "Momentum and Energy in the Wake of a Pigeon (*Columba livia*) in Slow Flight," *Journal of Experimental Biology*, Vol. 111, July 1984, pp. 81–102.

[8]Jones, K. D., Dohring, C. M., and Platzer, M. F., "Wake Structures Behind Plunging Airfoils: A Comparison of Numerical and Experimental Results," AIAA Paper 96-0078, Jan. 1996.

[9]Wilmott, P., "Unsteady Lifting-Line Theory by the Method of Matched Asymptotic Expansions," *Journal of Fluid Mechanics*, Vol. 186, Jan. 1988, pp. 303–320.

[10]Phlips, P. J., East, R. A., and Pratt, N. H., "An Unsteady Lifting Line Theory of Flapping Wings with Application to the Forward Flight of Birds," *Journal of Fluid Mechanics*, Vol. 112, Nov. 1981, pp. 97–125.

[11]Ahmadi, A. R., and Widnall, S. E., "Unsteady Lifting-Line Theory as a Singular-Perturbation Problem," *Journal of Fluid Mechanics*, Vol. 153, April 1985, pp. 59–81.

[12]Lan, C. E., "The Unsteady Quasi-Vortex-Lattice Method with Applications to Animal Propulsion," *Journal of Fluid Mechanics*, Vol. 93, Pt. 4, 1979, pp. 747–765.

[13]Betz, A., "Schraubenpropeller mit geringstem Energieverlust," Mit einem Zusatz von L. Prandtl, *Nachrichten von der Königlichen Gesellschaft der Wissenschaften zu Göttingen*, Mathematisch-physikalische Klasse, 1919, pp. 193–217.

[14]Goldstein, S., "On the Vortex Theory of Screw Propellers," *Proceedings of the Royal Society of London, Series A: Mathematical and Physical Sciences*, Vol. 123, No. 792, 1929, pp. 440–465.

[15]Jones, R. T., "Wing Flapping with Minimum Energy," *Aeronautical Journal*, Vol. 84, July 1980, pp. 214–217.

[16]Potze, W., and Sparenberg, J. A., "On the Efficiency of Optimum Finite Amplitude Sculling Propulsion," *International Shipbuilding Progress*, Vol. 30, No. 351, 1983, pp. 238–244.

[17]Hall, S. R., Yang, K. Y., and Hall, K. C., "Helicopter Rotor Lift Distributions for Minimum Induced Power Loss," *Journal of Aircraft*, Vol. 31, No. 4, 1994, pp. 837–845.

[18]Hall, K. C., and Hall, S. R., "Minimum Induced Power Requirements for Flapping Flight," *Journal of Fluid Mechanics*, Vol. 323, Sept. 1996, pp. 285–315.

[19]Sparenberg, J. A., *Hydrodynamic Propulsion and Its Optimization: Analytic Theory*, Kluwer Academic, Norwell, MA, 1995, pp. 216, 217.

[20]De Jong, K., "On the Optimization, Including Viscosity Effects, of Ship Screw Propellers with Optional End Plates (Part I)," *International Shipbuilding Progress*, Vol. 38, No. 414, 1991, pp. 115–156.

[21]De Jong, K., "On the Optimization, Including Viscosity Effects, of Ship Screw Propellers with Optional End Plates (Part II)," *International Shipbuilding Progress*, Vol. 38, No. 415, 1991, pp. 211–252.

[22]Ashley, H., and Landahl, M., *Aerodynamics of Wings and Bodies*, Addison–Wesley, Reading, MA, 1965, pp. 21–50.

[23]Abbot, I. H., Von Doenhoff, A. E., and Stivers, L. S., Jr., "Summary of Airfoil Data," NACA Rept. 824, 1945.

[24]Katz, J., and Plotkin, A., *Low-Speed Aerodynamics: From Wing Theory to Panel Methods*, McGraw–Hill, New York, 1991.

[25]Pierre, D. A., and Lowe, M. J., *Mathematical Programming via Augmented Lagrangians: An Introduction with Computer Programs*, Addison–Wesley, Reading, MA, 1975.

[26]Tucker, V. A., "Respiratory Exchange and Evaporative Water Loss in the Flying Budgerigar," *Journal of Experimental Biology*, Vol. 48, No. 1, 1968, pp. 67–87.

[27]Tucker, V. A., "Bird Metabolism During Flight: Evaluation of a Theory," *J. Exp. Biol.*, Vol. 58, No. 3, 1973, pp. 689–709.

[28]Tucker, V. A., "Metabolism During Flight in the Laughing Gull, *Larus atricilla*," *American Journal of Physiology*, Vol. 222, No. 2, 1972, pp. 237–245.